2024 IEEE International Conference on Robotics and Automation (ICRA 2024)
May 13-17, 2024. Yokohama, Japan

Singularity-Robust Prioritized Whole-Body Tracking and Interaction Control With Smooth Task Transitions

Xuwei Wu, Alin Albu-Schäffer, and Alexander Dietrich

***Abstract*— In this work, we propose a singularity-robust whole-body control framework that ensures smooth task transitions while maintaining strict priorities. The weighted generalized inverse is adopted to derive a hierarchical control law compatible with singular and redundant tasks. Moreover, a smooth activation matrix is proposed to continuously shape both null-space projectors and task-level control actions. Validation has been conducted in MATLAB/Simulink and MuJoCo simulations with Rollin' Justin.**

I. Introduction

Advanced whole-body controllers have been increasingly deployed on humanoids and mobile manipulators for applications in cluttered, human-shared environments. To exploit the high degrees of freedom (DOF) of such systems, whole-body control frameworks generally employ a hierarchical structure of tasks, assigned with either soft or strict priorities. A strict hierarchy is usually preferred when executing safety-critical tasks. This can be realized through various methods, including null-space projections [1]–[3], hierarchical quadratic programming (HQP) [4], [5], and prioritized model predictive control (MPC) [6]–[8]. Although optimization-based approaches are advantageous for incorporating inequality constraints, they often demand intensive computations due to the complex search problem [9], and it remains challenging to conduct formal analysis of their stability properties [10].

Among approaches using null-space projections, passivity-based methods [11]–[15] leverage the inherent passivity properties of robot dynamics to minimize decoupling compensation, thus enhancing robustness against model uncertainties [16]. Recent works have extended the regulation case [11] to the tracking case, achieving uniform asymptotic stability [12] as well as uniform exponential stability and passivity [15]. However, these approaches can only be applied in the absence of kinematic singularities and task conflicts, and they do not allow arbitrary task dimensions. Such limitations are addressed in [13] by utilizing the weighted generalized inverse (WGI) [17]. Nevertheless, both [13] and its adaptive version [14] are designed for pure motion control but not for interaction control. To ensure safe physical interactions with humans and the environment, desired interaction behavior of the robot must be integrated into control design.

Singular tasks or their specific directions can be disabled without affecting the control of higher-priority tasks [3], [18]. However, online modification of the task hierarchy may cause discontinuous control inputs during transitions [19]–[24]. For projection-based approaches, smooth activation functions [20], [21], [23] can be applied to mitigate discontinuous projector updates. Yet, selecting appropriate truncation thresholds for matrix decomposition and activation functions remains challenging, especially for hierarchies with tasks having different physical units of measurement.

This work was supported by the Bavarian Ministry of Economic Affairs, Regional Development and Energy (StMWi) within the project SMiLE2gether (LABAY102). The authors are with the Institute of Robotics and Mechatronics, German Aerospace Center (DLR), 82234 Wessling, Germany, and also with the School of Computation, Information and Technology, TUM, 80333 Munich, Germany (e-mail: xuwei.wu@dlr.de).

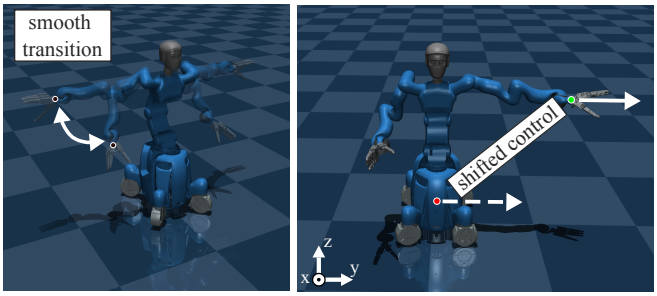

Fig. 1. Our approach ensures smooth task transitions during singularities (left) and shifts controllability of disabled tasks to lower-level ones while preserving the strict priorities of the remaining task hierarchy (right), as demonstrated in simulations with the humanoid robot Rollin' Justin.

In this work, we propose a singularity-robust whole-body tracking and interaction controller that ensures smooth task transitions during singularities while maintaining a strict hierarchy. Our approach extends previous works [12], [15] by using WGI-based null-space projectors, overcoming their aforementioned limitations, i.e., singularity-free operation and restricted task dimensions. Compared to [13], our approach can suitably handle physical interactions by design. It achieves decoupled interaction behavior for each task as in [15] and can account for external forces/torques from disabled tasks via null-space compliance. Additionally, we integrate a smooth activation matrix into the prioritized Jacobian and its WGI. A direct link between the singular values of the prioritized Jacobian and the eigenvalues of the task-space inertia is provided to facilitate an intuitive threshold selection. The proposed approach is validated via MATLAB/Simulink and MuJoCo simulations of the humanoid robot Rollin' Justin.

II. Preliminaries

A. Robot Dynamics and Task Hierarchy

Consider the rigid-body dynamics of a fully-actuated robot with n DOF:

$$\boldsymbol{M}(\boldsymbol{q})\ddot{\boldsymbol{q}} + \boldsymbol{C}(\boldsymbol{q},\dot{\boldsymbol{q}})\dot{\boldsymbol{q}} + \boldsymbol{g}(\boldsymbol{q}) = \boldsymbol{\tau} + \boldsymbol{\tau}^{\text{ext}} \ , \qquad (1)$$

where $\boldsymbol{q} \in \mathbb{R}^n$ describes the joint positions with time derivatives $\dot{\boldsymbol{q}}, \ddot{\boldsymbol{q}}$. The inertia matrix $\boldsymbol{M}(\boldsymbol{q})$ is symmetric positive

definite, and the Coriolis/centrifugal matrix $\boldsymbol{C}(\boldsymbol{q}, \dot{\boldsymbol{q}})$ satisfies the passivity property. Gravitational effects are denoted by $\boldsymbol{g}(\boldsymbol{q})$. System inputs include the actuator forces/torques $\boldsymbol{\tau}$ and the external ones $\boldsymbol{\tau}^{\text{ext}}$ exerted by the environment.

In prioritized multitask control, a robot executes $r \geq 2$ tasks simultaneously. Task i has a higher priority than task j if $i < j \leq r$. We denote the coordinate of task i and its time derivative as

$$\boldsymbol{x}_i \coloneqq \boldsymbol{f}_i(\boldsymbol{q}) \in \mathbb{R}^{m_i} \ , \quad \dot{\boldsymbol{x}}_i = \boldsymbol{J}_i(\boldsymbol{q})\dot{\boldsymbol{q}} \ , \tag{2}$$

where m_i is the task dimension, $\boldsymbol{f}_i : \mathbb{R}^n \to \mathbb{R}^{m_i}$ the differentiable map, and $\boldsymbol{J}_i(\boldsymbol{q}) \coloneqq \partial \boldsymbol{f}_i(\boldsymbol{q})/\partial \boldsymbol{q}$ the Jacobian matrix. The control goal for task i is to track a reference trajectory $\boldsymbol{x}_{i,\text{des}}(t), \dot{\boldsymbol{x}}_{i,\text{des}}(t), \ddot{\boldsymbol{x}}_{i,\text{des}}(t) \in \mathbb{R}^{m_i}$ over time t, while responding stably to the external force/torque $\boldsymbol{F}^{\text{ext}}_{\dot{\boldsymbol{x}}_i} \in \mathbb{R}^{m_i}$ collocated to $\dot{\boldsymbol{x}}_i$ with a desired impedance. Task errors are defined as $\tilde{\boldsymbol{x}}_i = \boldsymbol{x}_i - \boldsymbol{x}_{i,\text{des}}(t)$ with time derivatives $\dot{\tilde{\boldsymbol{x}}}_i$, $\ddot{\tilde{\boldsymbol{x}}}_i$. In the following, dependencies on $\boldsymbol{q}, \dot{\boldsymbol{q}}, t$ are omitted in the notations for the sake of simplicity.

B. Inertia-Weighted Pseudoinverse - The Nonsingular Case

Task priorities are maintained when the control input for task i, denoted by $\boldsymbol{\tau}_i \in \mathbb{R}^n$, does not interfere with the control goal of any higher-priority task during the transient. This can be achieved by projecting $\boldsymbol{\tau}_i$ onto the null space of $\boldsymbol{J}^{\text{aug}}_{i-1}\boldsymbol{M}^{-1}$, with the augmented Jacobian matrix defined as

$$\boldsymbol{J}^{\text{aug}}_{i-1} \coloneqq \begin{bmatrix} \boldsymbol{J}_1^T & \dots & \boldsymbol{J}_{i-1}^T \end{bmatrix}^T \in \mathbb{R}^{\sum_{j=1}^{i-1} m_j \times n} \ . \tag{3}$$

To this end, the null-space projector $\boldsymbol{N}_{i-1} \in \mathbb{R}^{n\times n}$ that ensures the dynamic consistency condition [25], [26]: $\boldsymbol{N}_{i-1}\boldsymbol{\tau}_i \in \text{null}(\boldsymbol{J}^{\text{aug}}_{i-1}\boldsymbol{M}^{-1})$, can be recursively computed by [3], [27]

$$\boldsymbol{N}_0 = \boldsymbol{I} \ ; \quad \boldsymbol{N}_i \coloneqq \boldsymbol{N}_{i-1} - \bar{\boldsymbol{J}}_i^T \bar{\boldsymbol{J}}_i^{M+,T} \tag{4}$$

for $i = 1, \dots, r$. Herein, $\bar{\boldsymbol{J}}_i \coloneqq \boldsymbol{J}_i\boldsymbol{N}_{i-1}^T \in \mathbb{R}^{m_i\times n}$ represents the prioritized Jacobian matrix, and

$$\bar{\boldsymbol{J}}_i^{M+} \coloneqq \boldsymbol{M}^{-1}\bar{\boldsymbol{J}}_i^T(\bar{\boldsymbol{J}}_i\boldsymbol{M}^{-1}\bar{\boldsymbol{J}}_i^T)^{-1} \in \mathbb{R}^{n\times m_i} \tag{5}$$

is the inertia-weighted pseudoinverse of $\bar{\boldsymbol{J}}_i$ [25]. When the stacked matrix $\bar{\boldsymbol{J}} \coloneqq \begin{bmatrix} \bar{\boldsymbol{J}}_1^T & \dots & \bar{\boldsymbol{J}}_r^T \end{bmatrix}^T$ is invertible, its inverse is given by [11]

$$\bar{\boldsymbol{J}}^{-1} = \begin{bmatrix} \bar{\boldsymbol{J}}_1^{M+} & \dots & \bar{\boldsymbol{J}}_r^{M+} \end{bmatrix} \ . \tag{6}$$

However, this requires: 1) $\sum_{i=1}^r m_i = n$; 2) $\boldsymbol{J}^{\text{aug}}_r$ is nonsingular. These conditions form the main limitations of the hierarchical controllers developed in [12], [15].

C. Weighted Generalized Inverse - The General Case

Indeed, $\bar{\boldsymbol{J}}_i^{M+}$ represents a special case of the WGI introduced in [17], which does not require $\bar{\boldsymbol{J}}_i$ to have full row rank. Given $\text{rank}(\bar{\boldsymbol{J}}_i) = p_i \leq m_i$, and a full-rank decomposition $\bar{\boldsymbol{J}}_i = \boldsymbol{F}_i\boldsymbol{G}_i$ where $\boldsymbol{F}_i \in \mathbb{R}^{m_i\times p_i}$, $\boldsymbol{G}_i \in \mathbb{R}^{p_i\times n}$, and $\text{rank}(\boldsymbol{F}_i) = \text{rank}(\boldsymbol{G}_i) = p_i$. The WGI of $\bar{\boldsymbol{J}}_i$ is given by [17]

$$\bar{\boldsymbol{J}}_i^{\#} \coloneqq \boldsymbol{W}_{\dot{\boldsymbol{q}}}^{-1}\boldsymbol{G}_i^T(\boldsymbol{G}_i\boldsymbol{W}_{\dot{\boldsymbol{q}}}^{-1}\boldsymbol{G}_i^T)^{-1}(\boldsymbol{F}_i^T\boldsymbol{W}_{\boldsymbol{v}_i}\boldsymbol{F}_i)^{-1}\boldsymbol{F}_i^T\boldsymbol{W}_{\boldsymbol{v}_i} \ , \tag{7}$$

where the metrics $\boldsymbol{W}_{\dot{\boldsymbol{q}}} \in \mathbb{R}^{n\times n}$ and $\boldsymbol{W}_{\boldsymbol{v}_i} \in \mathbb{R}^{m_i\times m_i}$ are symmetric positive definite matrices; the subscripts indicate the respective vector space of the metric. The vector $\boldsymbol{v}_i$ is obtained by the transformation $\boldsymbol{v}_i \coloneqq \bar{\boldsymbol{J}}_i\dot{\boldsymbol{q}}$. Apparently, if $p_i = m_i$, by choosing [28]

$$\boldsymbol{W}_{\dot{\boldsymbol{q}}} \coloneqq \boldsymbol{M} \ , \quad \boldsymbol{G}_i \coloneqq \bar{\boldsymbol{J}}_i \ , \quad \boldsymbol{W}_{\boldsymbol{v}_i} \coloneqq \boldsymbol{I} \ , \quad \boldsymbol{F}_i \coloneqq \boldsymbol{I}$$

we get $\bar{\boldsymbol{J}}_i^{\#} = \bar{\boldsymbol{J}}_i^{M+}$ (cf. (5)). When $\bar{\boldsymbol{J}}_i$ may not have full row rank, SVD and QR decomposition can be utilized to find a full-rank decomposition for $\bar{\boldsymbol{J}}_i$, see e. g. , [29, Appendix B] and [30, Appendix B].

Here, we briefly outline the formulation of $\boldsymbol{N}_i$ based on the SVD of weighted $\bar{\boldsymbol{J}}_i$. In this work, we assign $\boldsymbol{W}_{\dot{\boldsymbol{q}}} \coloneqq \boldsymbol{M}$ and $\boldsymbol{W}_{\boldsymbol{v}_i} \coloneqq \boldsymbol{I}$ such that the resulting $\boldsymbol{N}_i$ are equivalent to those in (4) in the absence of singularity. Given the Cholesky decomposition $\boldsymbol{W}_{\dot{\boldsymbol{q}}} = \boldsymbol{L}_{\dot{\boldsymbol{q}}}\boldsymbol{L}_{\dot{\boldsymbol{q}}}^T$, where $\boldsymbol{L}_{\dot{\boldsymbol{q}}} \in \mathbb{R}^{n\times n}$ is a lower triangular matrix with positive diagonal elements. The reduced SVD of $\bar{\boldsymbol{J}}_i\boldsymbol{L}_{\dot{\boldsymbol{q}}}^{-T}$ yields

$$\bar{\boldsymbol{J}}_i\boldsymbol{L}_{\dot{\boldsymbol{q}}}^{-T} = \boldsymbol{U}_i\boldsymbol{\Sigma}_i\boldsymbol{V}_i^T \implies \bar{\boldsymbol{J}}_i = \boldsymbol{U}_i\boldsymbol{\Sigma}_i\boldsymbol{V}_i^T\boldsymbol{L}_{\dot{\boldsymbol{q}}}^T \ , \tag{8}$$

where $\boldsymbol{U}_i \in \mathbb{R}^{m_i\times p_i}, \boldsymbol{\Sigma}_i \in \mathbb{R}^{p_i\times p_i}, \boldsymbol{V}_i \in \mathbb{R}^{n\times p_i}$ have rank p_i; $\boldsymbol{U}_i$ and $\boldsymbol{V}_i$ are orthogonal matrices. The diagonal matrix $\boldsymbol{\Sigma}_i \coloneqq \text{diag}\{\sigma_{i,k}\}$ with $k = 1, \dots, p_i$ contains the positive singular values $\sigma_{i,1} > \dots > \sigma_{i,p_i} > 0$. A valid full-rank decomposition of $\bar{\boldsymbol{J}}_i$ is obtained by[1] $\boldsymbol{F}_i \coloneqq \boldsymbol{U}_i$ and $\boldsymbol{G}_i \coloneqq \boldsymbol{\Sigma}_i\boldsymbol{V}_i^T\boldsymbol{L}_{\dot{\boldsymbol{q}}}^T$. Using this decomposition in (7) leads to

$$\bar{\boldsymbol{J}}_i^{\#} = \boldsymbol{L}_{\dot{\boldsymbol{q}}}^{-T}\boldsymbol{V}_i\boldsymbol{\Sigma}_i^{-1}\boldsymbol{U}_i^T \ . \tag{9}$$

Base on (8)–(9), the recursive step in (4) can be modified to

$$\boldsymbol{N}_i \coloneqq \boldsymbol{N}_{i-1} - \bar{\boldsymbol{J}}_i^T\bar{\boldsymbol{J}}_i^{\#,T} = \boldsymbol{N}_{i-1} - \boldsymbol{L}_{\dot{\boldsymbol{q}}}\boldsymbol{V}_i\boldsymbol{V}_i^T\boldsymbol{L}_{\dot{\boldsymbol{q}}}^{-1} \ . \tag{10}$$

The WGI with the chosen metrics has the properties [17]:

$$\bar{\boldsymbol{J}}_i\bar{\boldsymbol{J}}_i^{\#}\bar{\boldsymbol{J}}_i = \bar{\boldsymbol{J}}_i \ , \ \bar{\boldsymbol{J}}_i^{\#}\bar{\boldsymbol{J}}_i\bar{\boldsymbol{J}}_i^{\#} = \bar{\boldsymbol{J}}_i^{\#} \ , \ \bar{\boldsymbol{J}}_i\bar{\boldsymbol{J}}_i^{\#} = \bar{\boldsymbol{J}}_i^{\#,T}\bar{\boldsymbol{J}}_i^T \ . \tag{11}$$

The WGI of $\bar{\boldsymbol{J}}$ is given by $\bar{\boldsymbol{J}}^{\#} = \begin{bmatrix} \bar{\boldsymbol{J}}_1^{\#} & \dots & \bar{\boldsymbol{J}}_r^{\#} \end{bmatrix}$ [13].

D. Assumptions

We make the following assumptions:

Assumption 1: Redundant tasks can be designed such that $\sum_{i=1}^r m_i >= n$.

Assumption 2: $\bar{\boldsymbol{J}}$ always maintains full column rank, i.e., $\text{rank}(\bar{\boldsymbol{J}}) = n$.

Assumption 3: Measurements or estimations of $\boldsymbol{\tau}^{\text{ext}}$ and all $\boldsymbol{F}^{\text{ext}}_{\dot{\boldsymbol{x}}_i}$ are available.

Under Assumptions 1–2, the conditions $\bar{\boldsymbol{J}}^{\#}\bar{\boldsymbol{J}} = \boldsymbol{I}$ and $\bar{\boldsymbol{J}}\bar{\boldsymbol{J}}^{\#} = \text{diag}\{\bar{\boldsymbol{J}}_i\bar{\boldsymbol{J}}_i^{\#}\}$ hold [13]. Both assumptions are satisfied, when a n-DOF posture task is defined on the lowest level [31], [32]. To address Assumption 3, $\boldsymbol{F}^{\text{ext}}_{\dot{\boldsymbol{x}}_i}$ can[2] be measured by force/torque sensors mounted at the specified interaction locations, such as the end-effectors, or estimated by exploiting sensing redundancy [33]; $\boldsymbol{\tau}^{\text{ext}}$ can be estimated using the momentum-based observer [34].

[1]Note that for any $\boldsymbol{A} \in \mathbb{R}^{m\times n}$ and $\boldsymbol{B} \in \mathbb{R}^{n\times n}$, if $\text{rank}(\boldsymbol{B}) = n$, then $\text{rank}(\boldsymbol{AB}) = \text{rank}(\boldsymbol{A})$.

[2]When task r is defined as a n-DOF posture regulation task, $\boldsymbol{F}^{\text{ext}}_{\dot{\boldsymbol{x}}_r}$ can be designed to realize null-space compliance, as will be shown in Section IV-C.

III. Smooth Task Transitions Through Continuous Activation

A. Physically Intuitive Threshold in SVD

The SVD in (8) is typically truncated according to a manually selected threshold to prevent unbounded WGI. This can be challenging in practice, when the tasks have diverse physical units of measurement. In the following, we establish the relation between the singular values obtained in (8) and the eigenvalues of the task-space inertia, facilitating an intuitive and physically motivated threshold selection.

Performing the coordinate transformation $\dot{\boldsymbol{q}} = \bar{\boldsymbol{J}}^{\#}\boldsymbol{v}$ in (1) yields

$$\boldsymbol{\Lambda}\dot{\boldsymbol{v}} + \boldsymbol{\mu}\boldsymbol{v} = \bar{\boldsymbol{J}}^{\#,T}(\boldsymbol{\tau} + \boldsymbol{\tau}^{\text{ext}} - \boldsymbol{g}) \ , \tag{12a}$$

$$\boldsymbol{\Lambda} \coloneqq \bar{\boldsymbol{J}}^{\#,T}\boldsymbol{M}\bar{\boldsymbol{J}}^{\#} \ , \quad \boldsymbol{\mu} \coloneqq \bar{\boldsymbol{J}}^{\#,T}(\boldsymbol{C}\bar{\boldsymbol{J}}^{\#} + \boldsymbol{M}\dot{\bar{\boldsymbol{J}}}^{\#}) \ , \tag{12b}$$

where $\boldsymbol{\Lambda}$ and $\boldsymbol{\mu}$ are the task-space inertia and Coriolis/centrifugal matrix, respectively; $\boldsymbol{\Lambda} = \operatorname{diag}\{\boldsymbol{\Lambda}_i\}$ with $\boldsymbol{\Lambda}_i \coloneqq \bar{\boldsymbol{J}}_i^{\#,T}\boldsymbol{M}\bar{\boldsymbol{J}}_i^{\#} \in \mathbb{R}^{m_i \times m_i}$. The pseudoinverse of $\boldsymbol{\Lambda}_i$ is defined as $\boldsymbol{\Lambda}_i^{\#} \coloneqq \bar{\boldsymbol{J}}_i \boldsymbol{M}^{-1}\bar{\boldsymbol{J}}_i^T$ [35]. Using (8)–(9), we obtain

$$\boldsymbol{\Lambda}_i = \boldsymbol{U}_i\boldsymbol{\Sigma}_i^{-2}\boldsymbol{U}_i^T \ , \quad \boldsymbol{\Lambda}_i^{\#} = \boldsymbol{U}_i\boldsymbol{\Sigma}_i^{2}\boldsymbol{U}_i^T \ , \tag{13}$$

where $\boldsymbol{\Sigma}_i^2 = \operatorname{diag}\{\sigma_{i,k}^2\}$ and $\boldsymbol{\Sigma}_i^{-2}$ is its inverse. It can be straightforwardly verified that

$$\boldsymbol{\Lambda}_i\boldsymbol{\Lambda}_i^{\#} = \bar{\boldsymbol{J}}_i\bar{\boldsymbol{J}}_i^{\#} \ , \ \boldsymbol{\Lambda}_i\boldsymbol{\Lambda}_i^{\#}\boldsymbol{\Lambda}_i = \boldsymbol{\Lambda}_i \ , \ \boldsymbol{\Lambda}_i^{\#}\boldsymbol{\Lambda}_i\boldsymbol{\Lambda}_i^{\#} = \boldsymbol{\Lambda}_i^{\#} \ . \tag{14}$$

Let $\bar{\boldsymbol{U}}_i \in \mathbb{R}^{m_i \times (m_i - p_i)}$ denote the orthogonal complement of $\boldsymbol{U}_i$, the eigen-decomposition of $\boldsymbol{\Lambda}_i$ can be written as [3]

$$\boldsymbol{\Lambda}_i = \begin{bmatrix}\boldsymbol{U}_i & \bar{\boldsymbol{U}}_i\end{bmatrix}\begin{bmatrix}\boldsymbol{\Sigma}_i^{-2} & \\ & \boldsymbol{0}\end{bmatrix}\begin{bmatrix}\boldsymbol{U}_i^T \\ \bar{\boldsymbol{U}}_i^T\end{bmatrix} \ . \tag{15}$$

Therefore, $\lambda_{i,k} \coloneqq 1/\sigma_{i,k}^2$ with $k = 1, \dots, p_i$ are the nonzero eigenvalues of $\boldsymbol{\Lambda}_i$. The columns of $\boldsymbol{U}_i$ corresponding to large eigenvalues in (15) indicate uncontrollable directions near singularities [3], [18]. Hence, the truncation threshold δ_i of the singular values $[\sigma_{i,1}, \dots, \sigma_{i,p_i}]$ is equivalent to the inverse square root of the maximum allowable eigenvalue of $\boldsymbol{\Lambda}_i$. This insight enables a more physically meaningful selection of δ_i based on task inertia properties. For example, δ_i can be chosen to limit the achievable reflected mass of a Cartesian task for ensuring collision safety [36], [37].

On the other hand, applying truncated SVD in (8) yields an approximated WGI. This approximation is considered negligible in the literature, as δ_i is usually set close to machine precision. However, when δ_i is chosen with more physical relevance, as suggested in this work, it may affect the block-diagonal structure[3] of $\bar{\boldsymbol{J}}\bar{\boldsymbol{J}}^{\#}$, which is crucial for the controller design in Section IV-B. Therefore, $\bar{\boldsymbol{J}}_i$ should be substituted by $\boldsymbol{U}_i\boldsymbol{\Sigma}_i\boldsymbol{V}_i^T\boldsymbol{L}_{\dot{\boldsymbol{q}}}^T$ *after* performing the truncated SVD. This substitution is incorporated into the smooth transition strategy, as will be shown in Section III-B.

Remark 1: Although the eigen-decomposition (15) has been presented in [3], a direct relation to the SVD truncation thresholds was not provided.

[3] $\bar{\boldsymbol{J}}\bar{\boldsymbol{J}}^{\#}$ may then have nonzero entries in its upper triangular blocks.

B. Smooth Task Transitions

Another issue with truncated SVD is the sudden change of subspaces when a singular value is crossing the threshold, causing discontinuous control actions. In [20], an activation matrix was introduced to realize smooth transitions of the projectors. We extend this concept by integrating the activation matrix into both $\bar{\boldsymbol{J}}_i$ and $\bar{\boldsymbol{J}}_i^{\#}$ to smoothly shape the task-level control action. The activation matrix is defined as

$$\boldsymbol{A}_i \coloneqq \operatorname{diag}\{a_i(\sigma_{i,k})\} \ , \forall k = 1, \dots, p_i \ . \tag{16}$$

We choose each activation function $a_i : \mathbb{R}_+ \to [0, 1]$ as [38]

$$a_i(\sigma_{i,k}) \coloneqq \begin{cases} 0 & \sigma_{i,k} < \delta_i - h_i \\ 6\Delta_i^5 - 15\Delta_i^4 + 10\Delta_i^3 & \delta_i - h_i \le \sigma_{i,k} \le \delta_i \\ 1 & \delta_i < \sigma_{i,k} \end{cases} \tag{17}$$

with $0 < h_i < \delta_i$ and $\Delta_i \coloneqq (\sigma_{i,k} - \delta_i + h_i)/h_i$. The fifth-order polynomial ensures zero first and second derivatives at the boundaries. Finally, we integrate this activation matrix into the computation of $\bar{\boldsymbol{J}}_i$, $\bar{\boldsymbol{J}}_i^{\#}$, and $\boldsymbol{N}_i$ as

$$\bar{\boldsymbol{J}}_i \coloneqq \boldsymbol{U}_i\boldsymbol{A}_i\boldsymbol{\Sigma}_i\boldsymbol{V}_i^T\boldsymbol{L}_{\dot{\boldsymbol{q}}}^T, \ \bar{\boldsymbol{J}}_i^{\#} \coloneqq \boldsymbol{L}_{\dot{\boldsymbol{q}}}^{-T}\boldsymbol{V}_i\boldsymbol{A}_i\boldsymbol{\Sigma}_i^{-1}\boldsymbol{U}_i^T, \tag{18a}$$

$$\boldsymbol{N}_i \coloneqq \boldsymbol{N}_{i-1} - \boldsymbol{L}_{\dot{\boldsymbol{q}}}\boldsymbol{V}_i\boldsymbol{A}_i\boldsymbol{V}_i^T\boldsymbol{L}_{\dot{\boldsymbol{q}}}^{-1} \ . \tag{18b}$$

IV. Singularity-Robust Whole-Body Tracking and Interaction Control

A. Coordinate Transformation

As in [12], [15], we develop a control law formulated in the original task-space variables $\boldsymbol{x}$ and $\dot{\boldsymbol{x}}$. This requires the determination of the transformation from $\dot{\boldsymbol{x}}$ to $\boldsymbol{v}$, denoted by[4] $\boldsymbol{v} = \boldsymbol{B}\dot{\boldsymbol{x}}$. In [13], the matrix $\boldsymbol{T} \in \mathbb{R}^{\sum_{i=1}^r m_i \times \sum_{i=1}^r m_i}$ of the inverse transformation $\dot{\boldsymbol{x}} = \boldsymbol{T}\boldsymbol{v}$ has been derived as

$$\boldsymbol{T} = \begin{bmatrix} \boldsymbol{I} & \boldsymbol{0} & \boldsymbol{0} & \dots & \boldsymbol{0} \\ \boldsymbol{J}_2\bar{\boldsymbol{J}}_1^{\#} & \boldsymbol{I} & \boldsymbol{0} & \dots & \boldsymbol{0} \\ \dots & \dots & \dots & \dots & \boldsymbol{0} \\ \boldsymbol{J}_r\bar{\boldsymbol{J}}_1^{\#} & \boldsymbol{J}_r\bar{\boldsymbol{J}}_2^{\#} & \dots & \dots & \boldsymbol{I} \end{bmatrix} \ . \tag{19}$$

Since $\boldsymbol{T}$ is invertible [13], we have $\boldsymbol{B} = \boldsymbol{T}^{-1}$. Thus, $\boldsymbol{B}$ features a lower block-triangular structure with identity matrices on the diagonal. The following proposition establishes the analytical expression of the lower triangular blocks of $\boldsymbol{B}$.

Proposition 1: The (i, j)-block of $\boldsymbol{B}$ for $i > j$ is given by

$$\boldsymbol{B}_{i,j} = -\boldsymbol{J}_i\boldsymbol{\Phi}_{i,j}\bar{\boldsymbol{J}}_j^{\#} \in \mathbb{R}^{m_i \times m_j} \ , \ \boldsymbol{\Phi}_{i,j} \coloneqq \prod_{k=j+1}^{i-1} \boldsymbol{I} - \bar{\boldsymbol{J}}_k^{\#}\boldsymbol{J}_k \ , \tag{20}$$

where $\boldsymbol{\Phi}_{i,i-1} = \boldsymbol{I}$, and $\prod$ is the left matrix multiplication.

Proof: Based on (19), it can be verified that $\boldsymbol{v}_i = \dot{\boldsymbol{x}}_i - \boldsymbol{J}_i\sum_{j=1}^{i-1}\bar{\boldsymbol{J}}_j^{\#}\boldsymbol{v}_j$ for $i = 2, \dots, r$. The proof follows directly from the induction in [15, Appendix B]. ■

By leveraging the structure of $\boldsymbol{T}$, we develop an efficient iterative algorithm for computing $\boldsymbol{B}$, as presented in Appendix.

[4] Note that the derivation of $\boldsymbol{B}$ in [15] requires $\boldsymbol{J}_r^{\text{aug}}$ to be invertible.

B. Control Law

Since task transitions are typically faster than the system dynamics, as indicated in [20], we assume that the activation matrix $\boldsymbol{A}_i$ only has entries of 1 or 0 in the following. Thus, the properties from (11) are preserved for the shaped matrices in (18a). The control law is expressed as

$$\boldsymbol{\tau} = \boldsymbol{g} + \boldsymbol{\tau}_{\boldsymbol{\mu}} + \sum_{i=1}^{r} \bar{\boldsymbol{J}}_i^T \boldsymbol{F}_{i,\mathrm{ctrl}} \ . \tag{21}$$

Here, $\boldsymbol{\tau}_{\boldsymbol{\mu}} \coloneqq \bar{\boldsymbol{J}}^T(\boldsymbol{\mu} - \bar{\boldsymbol{\mu}})\boldsymbol{v}$ with $\bar{\boldsymbol{\mu}}$ containing the main-diagonal blocks extracted from $\boldsymbol{\mu}$. Thus, $\boldsymbol{\tau}_{\boldsymbol{\mu}}$ compensates for the cross-couplings within $\boldsymbol{\mu}\boldsymbol{v}$ [11]. The term $\boldsymbol{F}_{i,\mathrm{ctrl}} \in \mathbb{R}^{m_i}$ represents the task-level control law to be designed. Applying (21) to (12a), while considering (11) and the block-diagonal structure of $\boldsymbol{\Lambda}$, $\bar{\boldsymbol{\mu}}$, and $\bar{\boldsymbol{J}}\bar{\boldsymbol{J}}^{\#}$, we can express the dynamics of each task separately as

$$\boldsymbol{\Lambda}_i \dot{\boldsymbol{v}}_i + \boldsymbol{\mu}_i \boldsymbol{v}_i = \bar{\boldsymbol{J}}_i^{\#,T} \bar{\boldsymbol{J}}_i^T \boldsymbol{F}_{i,\mathrm{ctrl}} + \bar{\boldsymbol{J}}_i^{\#,T} \boldsymbol{\tau}^{\mathrm{ext}} \tag{22}$$

for $i = 1, \ldots, r$, where $\boldsymbol{\mu}_i$ is the i-th diagonal block of $\bar{\boldsymbol{\mu}}$. The task-level control law is designed as

$$\boldsymbol{F}_{i,\mathrm{ctrl}} \coloneqq \boldsymbol{F}_{i,\mathrm{ff}} + \boldsymbol{F}_{i,\mathrm{imp}} + \boldsymbol{F}_{i,\mathrm{comp}}^{\mathrm{dyn}} + \boldsymbol{F}_{i,\mathrm{comp}}^{\mathrm{ext}} \ , \tag{23a}$$

$$\boldsymbol{F}_{i,\mathrm{ff}} \coloneqq \boldsymbol{\Lambda}_i \ddot{\boldsymbol{x}}_{i,\mathrm{des}} + \boldsymbol{\mu}_i \dot{\boldsymbol{x}}_{i,\mathrm{des}} \ , \tag{23b}$$

$$\boldsymbol{F}_{i,\mathrm{imp}} \coloneqq -\boldsymbol{K}_i \tilde{\boldsymbol{x}}_i - \boldsymbol{D}_i \dot{\tilde{\boldsymbol{x}}}_i \ , \tag{23c}$$

$$\boldsymbol{F}_{i,\mathrm{comp}}^{\mathrm{dyn}} \coloneqq \boldsymbol{\Lambda}_i \sum_{j=1}^{i-1} \left(\boldsymbol{B}_{i,j} \ddot{\boldsymbol{x}}_{j,\mathrm{ref}} + \dot{\boldsymbol{B}}_{i,j} \dot{\boldsymbol{x}}_j \right) + \boldsymbol{\mu}_i \sum_{j=1}^{i-1} \boldsymbol{B}_{i,j} \dot{\boldsymbol{x}}_j \ , \tag{23d}$$

$$\boldsymbol{F}_{i,\mathrm{comp}}^{\mathrm{ext}} \coloneqq \bar{\boldsymbol{J}}_i^{\#,T} \bar{\boldsymbol{J}}_i^T \boldsymbol{F}_{\dot{\boldsymbol{x}}_i}^{\mathrm{ext}} - \bar{\boldsymbol{J}}_i^{\#,T} \boldsymbol{\tau}^{\mathrm{ext}} \ . \tag{23e}$$

As in [15], the terms (23b)–(23e) correspond to the feed-forward control, the proportional-derivative (PD) control, the dynamics decoupling ($\boldsymbol{F}_{1,\mathrm{comp}}^{\mathrm{dyn}} = \boldsymbol{0}$), and the external force/torque decoupling, respectively. The stiffness and damping matrices are defined as $\boldsymbol{K}_i = \boldsymbol{\Lambda}_i \boldsymbol{\Lambda}_i^{\#} \bar{\boldsymbol{K}}_i \boldsymbol{\Lambda}_i \boldsymbol{\Lambda}_i^{\#}$ and $\boldsymbol{D}_i = \boldsymbol{\Lambda}_i \boldsymbol{\Lambda}_i^{\#} \bar{\boldsymbol{D}}_i \boldsymbol{\Lambda}_i \boldsymbol{\Lambda}_i^{\#}$, respectively; $\bar{\boldsymbol{K}}_i$ and $\bar{\boldsymbol{D}}_i$ are suppose to be symmetric positive definite. This definition ensures that $\boldsymbol{K}_i$ and $\boldsymbol{D}_i$ comply with the controllable task directions [18]. The reference acceleration $\ddot{\boldsymbol{x}}_{j,\mathrm{ref}}$ is defined as

$$\ddot{\boldsymbol{x}}_{j,\mathrm{ref}} \coloneqq \ddot{\boldsymbol{x}}_{j,\mathrm{des}} + \boldsymbol{\Lambda}_j^{\#} \left(\boldsymbol{F}_{\dot{\boldsymbol{x}}_j}^{\mathrm{ext}} - (\boldsymbol{\mu}_j + \boldsymbol{D}_j) \dot{\tilde{\boldsymbol{x}}}_j - \boldsymbol{K}_j \tilde{\boldsymbol{x}}_j \right) \tag{24}$$

for $1 \leq j < r$. The main advantage of the proposed control law over [15] is its compatibility with rank-deficient $\bar{\boldsymbol{J}}_i$.

Applying (23) to (22) and considering the properties (11), (14), we obtain

$$\boldsymbol{\Lambda}_i (\ddot{\tilde{\boldsymbol{x}}}_i + \boldsymbol{\gamma}_i) + \boldsymbol{\mu}_i \dot{\tilde{\boldsymbol{x}}}_i + \boldsymbol{D}_i \dot{\tilde{\boldsymbol{x}}}_i + \boldsymbol{K}_i \tilde{\boldsymbol{x}}_i = \boldsymbol{\Lambda}_i \boldsymbol{\Lambda}_i^{\#} \boldsymbol{F}_{\dot{\boldsymbol{x}}_i}^{\mathrm{ext}} \tag{25}$$

for $i = 1, \ldots, r$, where $\boldsymbol{\gamma}_i$ denotes the top-down disturbances

$$\boldsymbol{\gamma}_1 = \boldsymbol{0} \ ; \ \boldsymbol{\gamma}_i \coloneqq \sum_{j=1}^{i-1} \boldsymbol{B}_{i,j} (\ddot{\boldsymbol{x}}_j - \ddot{\boldsymbol{x}}_{j,\mathrm{ref}}) \ , \ \ \forall i = 2, \ldots, r \ . \tag{26}$$

The following proposition justifies that $\boldsymbol{\gamma}_i$ is indeed canceled out through $\boldsymbol{F}_{i,\mathrm{comp}}^{\mathrm{dyn}}$, even if higher-level tasks may lose rank.

Proposition 2: Under Assumption 3, the disturbance term $\boldsymbol{\gamma}_i$ vanishes for $i = 2, \ldots, r$.

Proof: With ideal external force/torque decoupling, task 1 achieves the desired closed-loop dynamics (25). Pre-multiplying it with $\bar{\boldsymbol{J}}_1^{\#} \boldsymbol{\Lambda}_1^{\#}$ and using (11), (14), (24) we obtain $\bar{\boldsymbol{J}}_1^{\#} (\ddot{\boldsymbol{x}}_1 - \ddot{\boldsymbol{x}}_{1,\mathrm{ref}}) = \boldsymbol{0}$. By using (20), it follows that

$$\boldsymbol{B}_{i,1} (\ddot{\boldsymbol{x}}_1 - \ddot{\boldsymbol{x}}_{1,\mathrm{ref}}) = -\boldsymbol{J}_i \boldsymbol{\Phi}_{i,1} \bar{\boldsymbol{J}}_1^{\#} (\ddot{\boldsymbol{x}}_1 - \ddot{\boldsymbol{x}}_{1,\mathrm{ref}}) = \boldsymbol{0} \tag{27}$$

holds for $i = 2, \ldots, r$. The proof can be established in a cascaded manner by starting from task $j = 2$ and showing

$$\boldsymbol{\gamma}_j = \boldsymbol{0} \implies \boldsymbol{B}_{i,j} (\ddot{\boldsymbol{x}}_j - \ddot{\boldsymbol{x}}_{j,\mathrm{ref}}) = \boldsymbol{0} \ , \forall i = j+1, \ldots, r \tag{28}$$

which leads to the precondition $\boldsymbol{\gamma}_{j+1} = \boldsymbol{0}$ for the subsequent step. Note that $\boldsymbol{\gamma}_2 = \boldsymbol{0}$ follows directly from (27). ∎

Finally, under Proposition 2, the closed-loop dynamics of task i are given by

$$\boldsymbol{\Lambda}_i \ddot{\tilde{\boldsymbol{x}}}_i + \boldsymbol{\mu}_i \dot{\tilde{\boldsymbol{x}}}_i + \boldsymbol{D}_i \dot{\tilde{\boldsymbol{x}}}_i + \boldsymbol{K}_i \tilde{\boldsymbol{x}}_i = \boldsymbol{\Lambda}_i \boldsymbol{\Lambda}_i^{\#} \boldsymbol{F}_{\dot{\boldsymbol{x}}_i}^{\mathrm{ext}} \ . \tag{29}$$

When $\bar{\boldsymbol{J}}_i$ has full row rank (i. e., $\boldsymbol{\Lambda}_i \boldsymbol{\Lambda}_i^{\#} = \boldsymbol{I}$), (29) reduces to the closed-loop dynamics in [15]. If this holds for all tasks and $\sum_{i=1}^{r} m_i = n$, the proposed controller simplifies[5] to [15] and inherits its stability and passivity properties.

Remark 2: Despite the proposed smooth transition strategy in Section III-B, we still observe discontinuities in terms involving $\boldsymbol{\mu}$, that is, $\boldsymbol{\tau}_{\boldsymbol{\mu}}$, and at the task level, $\boldsymbol{F}_{i,\mathrm{ff}}$ and $\boldsymbol{F}_{i,\mathrm{comp}}^{\mathrm{dyn}}$, especially for high-dimensional tasks with frequent rank changes. This occurs because SVD cannot guarantee continuous factorization for matrices with changing ranks [39], and computing $\boldsymbol{\mu}$ requires the numerical differentiation of $\bar{\boldsymbol{J}}^{\#}$. For practical implementation, we recommend: 1) using advanced filtering techniques for $\boldsymbol{\mu}$; 2) disabling $\boldsymbol{F}_{r,\mathrm{ff}}$ and $\boldsymbol{F}_{r,\mathrm{comp}}^{\mathrm{dyn}}$ of task r, thus making it an impedance-based regulation task. The modification preserves the ability of task r to ensure stable and compliant behavior at singularities.

C. Null-Space Compliance on the Lowest Level

Given a n-DOF posture task on the lowest level, we can use its compliance to appropriately manage interaction forces/torques from disabled (parts of) higher-level tasks. Under Assumption 3, this is achieved by assigning

$$\boldsymbol{F}_{\dot{\boldsymbol{x}}_r}^{\mathrm{ext}} \coloneqq \boldsymbol{\tau}^{\mathrm{ext}} - \sum_{i=1}^{r-1} \boldsymbol{J}_i^T \boldsymbol{\Lambda}_i \boldsymbol{\Lambda}_i^{\#} \boldsymbol{F}_{\dot{\boldsymbol{x}}_i}^{\mathrm{ext}} \tag{30}$$

in (23e) for task r, while $\boldsymbol{\tau}^{\mathrm{ext}}$ and $\boldsymbol{F}_{\dot{\boldsymbol{x}}_i}^{\mathrm{ext}}$ for $i = 1, \ldots, r-1$ are estimated or measured. Let $\boldsymbol{\tau}_{\mathrm{res}}^{\mathrm{ext}}$ denote the residual external forces/torques in joint space that are not attributed to any higher-level task, such that[6]

$$\boldsymbol{\tau}^{\mathrm{ext}} - \boldsymbol{\tau}_{\mathrm{res}}^{\mathrm{ext}} = \sum_{i=1}^{r-1} \boldsymbol{J}_i^T \boldsymbol{F}_{\dot{\boldsymbol{x}}_i}^{\mathrm{ext}} \ . \tag{31}$$

Then, (30) can be reformulated as

$$\boldsymbol{F}_{\dot{\boldsymbol{x}}_r}^{\mathrm{ext}} = \boldsymbol{\tau}_{\mathrm{res}}^{\mathrm{ext}} + \sum_{i=1}^{r-1} \boldsymbol{J}_i^T (\boldsymbol{I} - \boldsymbol{\Lambda}_i \boldsymbol{\Lambda}_i^{\#}) \boldsymbol{F}_{\dot{\boldsymbol{x}}_i}^{\mathrm{ext}} \ . \tag{32}$$

Thus, $\boldsymbol{F}_{\dot{\boldsymbol{x}}_r}^{\mathrm{ext}}$ accounts for both $\boldsymbol{\tau}_{\mathrm{res}}^{\mathrm{ext}}$ and the interaction forces/torques in the disabled directions of all higher-level tasks, which will otherwise be fully compensated via (23e).

[5] In this case, a posture task on the lowest-priority level is not needed.

[6] The external forces/torques of redundant tasks, i.e., $\boldsymbol{J}_i = \boldsymbol{J}_j$ with $i \neq j$, are only considered once in the sum on the right-hand side of (31).

TABLE I

CONTROLLER GAINS FOR SIMULATION #1

Task	Stiffness / Damping
1	(400, 400) $\frac{\text{N}}{\text{m}}$, 100 $\frac{\text{Nm}}{\text{rad}}$ / (100, 100) $\frac{\text{Ns}}{\text{m}}$, 40 $\frac{\text{Nms}}{\text{rad}}$
2/4	(1000, 1000, 1000) $\frac{\text{N}}{\text{m}}$ / (100, 100, 100) $\frac{\text{Ns}}{\text{m}}$
3/5	(100, 100, 100) $\frac{\text{Nm}}{\text{rad}}$ / (30, 30, 30) $\frac{\text{Nms}}{\text{rad}}$
6	(200, 200) $\frac{\text{N}}{\text{m}}$, (50, 150*) $\frac{\text{Nm}}{\text{rad}}$ / (50, 50) $\frac{\text{Ns}}{\text{m}}$, (20, 20*) $\frac{\text{Nms}}{\text{rad}}$

* For all 17 upper-body joints.

V. SIMULATION VALIDATIONS

The proposed approach has been validated in two simulations with Rollin' Justin, a humanoid robot featuring 17 torque-controlled DOF in the upper body and a 3-DOF velocity-controlled mobile platform. An admittance interface [40] is employed to transform virtual force/torque commands of the whole-body controller into desired velocities for the platform's kinematic controller [41]. The robot model is simulated in MuJoCo [42], while the control algorithms are implemented in MATLAB/Simulink, both updated at a time step of 1 ms. The task hierarchy consists of six priority levels:

1) Position and orientation of the platform ($m_1 = 3$);
2) Translational impedance at the right tool center point (TCP) ($m_2 = 3$);
3) Rotational impedance at the right TCP ($m_3 = 3$);
4) Translational impedance at the left TCP ($m_4 = 3$);
5) Rotational impedance at the left TCP ($m_5 = 3$);
6) Position and orientation of the platform[7], and joint impedance at all upper-body joints ($m_6 = 20$).

The trajectories for tasks 1-5 are obtained through forward kinematics by using the joint-space trajectories[8] of task 6; all trajectories are thus inherently compatible. According to Remark 2, the high-pass rate limiter from [44] is applied to filter the task-space Coriolis/centrifugal matrix. Also, the feedforward and dynamics decoupling terms for task 6 are deactivated, as this task is intended for joint-space regulation during singularities. For both simulations, the default SVD truncation thresholds are set to $[0.04,\ 0.04,\ 1,\ 0.04,\ 1,\ 0.1]^{1/2}$ for tasks 1-6, respectively. The chosen thresholds limit the reflected mass at each TCP to 25 kg and the reflected inertia to 1 kgm^2. In the second simulation, the thresholds for tasks 1, 4, and 5 are multiplied by 50 at certain times to intentionally disable these tasks. The parameter h_i in (17) is chosen as $h_i = 0.4\,\delta_i$ for all tasks. Preliminary simulations suggest $0.2\,\delta_i \leq h_i \leq 0.7\,\delta_i$ for balanced transition behavior between control smoothness and tracking performance.

A. Simulation #1: Tracking Trajectories With Singularities

The first simulation demonstrates the smooth transition behavior achieved by our approach in the presence of singularities. A circular trajectory is assigned to the platform

[7]The redundant task definition for the platform allows switching priorities without modifying the hierarchical structure, such as switching to task 1 for platform collision avoidance and to task 6 for mobile impedance.

[8]In practice, coordinated whole-body joint motions are typically generated by a high-level planner that checks for collisions and joint limits [43]. Cartesian impedance tasks 2-5 are necessary for handling physical interactions and achieving desired convergence properties in task space.

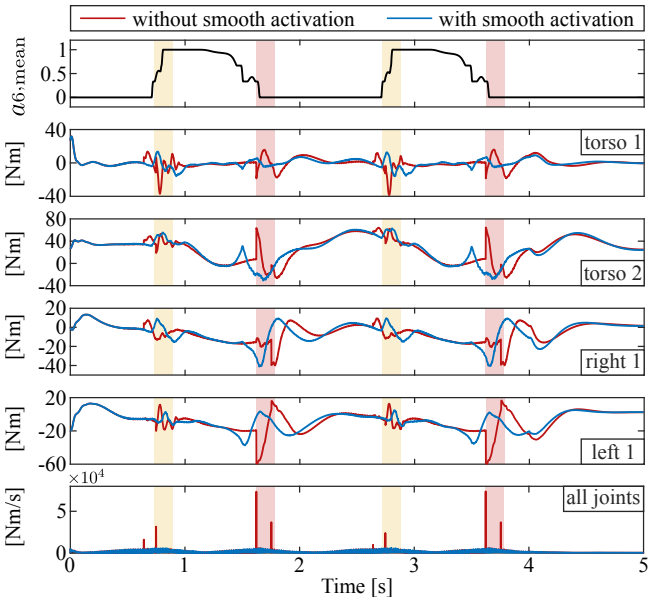

Fig. 2. Simulation #1. Top diagram: mean value of the varying activation functions of task 6. Middle diagrams: control torques for torso joints 1 and 2, right arm joint 1, and left arm joint 1. Bottom diagram: Euclidean norm of the numerical differentiation of all upper-body joints' control torques. The yellow shaded areas indicate the transfer of controllability from tasks 2 and 4 to task 6, while the red ones mark the reverse transition.

tasks on levels 1 and 6, while the trajectories for both arms pass through singular configurations, as shown in Fig. 1 (left). The control parameters are detailed in Table I. Also, initial position errors are introduced at all upper-body joints. Fig. 2 illustrates the variations in activation functions of task 6, the control torques of the selected joints[9], and the Euclidean norm of the numerical differentiation of all upper-joints' control torques. As highlighted, the proposed strategy effectively prevents discontinuous control commands during task transitions. Fig. 3 shows the Euclidean norms of the task position errors. The yellow rectangles mark the time intervals when tasks 2 and 4 are singular. One can observe that the proposed smooth transition strategy does not have a noticeable negative influence on the tracking performance.

B. Simulation #2: Physical Interactions With Disabled Tasks

In this simulation, the robot undergoes various physical interactions across the hierarchy, while tasks 1, 4, and 5 are disabled at certain times. The left arm follows the same trajectory as in Simulation #1. The platform and the right arm are commanded to maintain their initial configurations. The gains for tasks 2-5 are reduced by half of those in Table I for more compliance. At $t = 0$ s, task 1 is disabled, shifting the control of the platform's DOF to lower-level tasks. At $t = 4.5$ s, task 1 is enabled, while tasks 4 and 5 are disabled. Correspondingly, the simulation is divided into two phases:

- Phase #1 ($t = 0{\sim}4$ s): A 50 N external force applied at the left TCP (task 4) along the y-axis[10].
- Phase #2 ($t = 5{\sim}10$ s): 50 N external forces applied at the right TCP (tasks 2) along the x- and z-axes and a 30 Nm torque at the left TCP (task 5) about the z-axis.

[9]Because they are most significantly involved in task transitions.

[10]All task-space external force/torques are represented in the world frame.

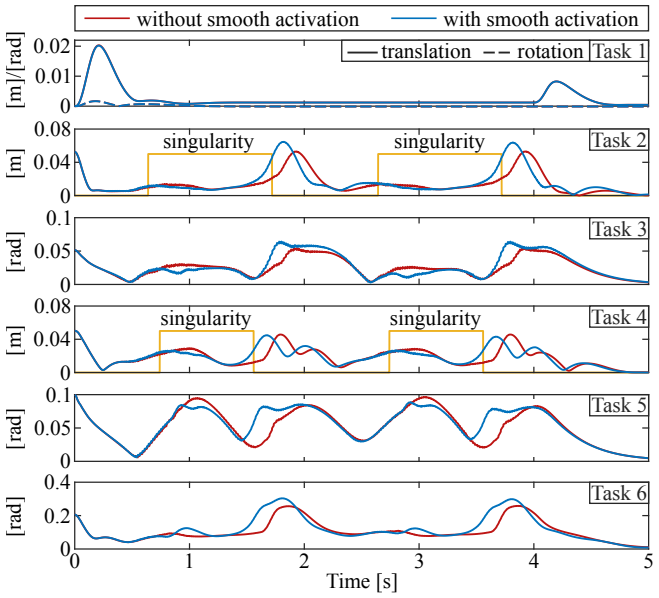

Fig. 3. Simulation #1. Euclidean norms of task position errors. The orientation errors at the TCP (tasks 3 and 5) are represented by the absolute angles between the actual and the desired frames. The bottom diagram only considers the errors of the upper-body joints. The initial and final position errors of the platform result from the initial and termination steering phases of the platform controller [41].

Fig. 4 shows the applied interactions and the task position errors. Snapshots of Phase #1 are provided in Fig. 5. Unlike in Simulation #1, task 4 does not encounter singularities in Phase #1 due to task 1 being disabled. Moreover, task 4 achieves its desired impedance, as evident in diagram 6 (left) of Fig. 4 and the snapshots. In Phase #2, although task 5 is disabled, the robot responds compliantly to the external torque at the left TCP owing to null-space compliance, as seen in the bottom diagram (right) and the accompanying video. Throughout this simulation, the desired interaction behaviors of tasks 2 and 3 remain undisturbed, demonstrating the effective external force/torque decoupling in task space.

VI. Conclusion

This paper presented a strictly prioritized whole-body tracking and interaction controller that achieves smooth task transitions during singularities. The limitations of previous works on singularity-free operation and overall task dimension have been eliminated by utilizing WGI-based null-space projectors. An activation matrix was applied to smoothly shape the prioritized Jacobian matrix and its WGI. Under physical interactions across the hierarchy, the proposed approach effectively decouples external forces/torques in task space. Validation has been carried out in MATLAB/Simulink and MuJoCo simulations. Future work will involve conducting formal passivity analysis, developing methods for handling SVD discontinuities caused by rank changes, and performing real robot experiments.

Appendix

Algorithm 1 is inspired by the inverse of a 2-by-2 lower triangular-block matrix with invertible diagonal blocks:

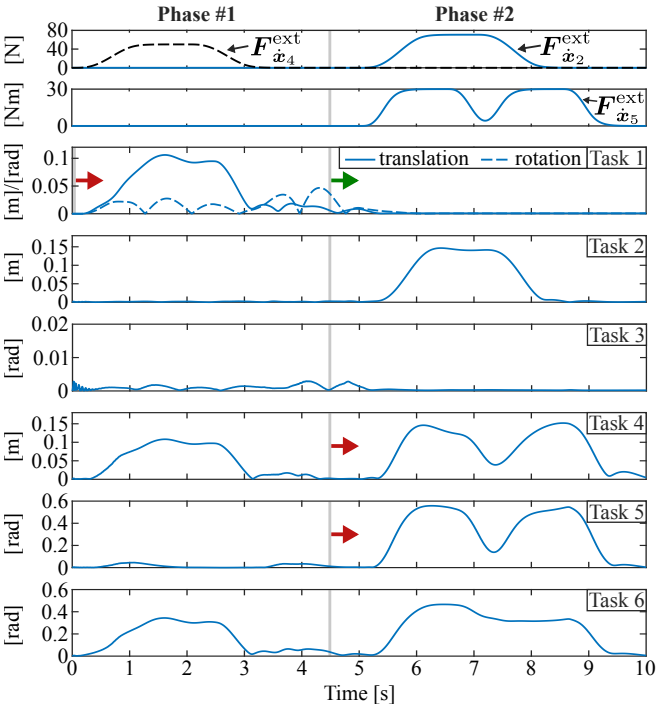

Fig. 4. Simulation #2. Diagrams 1-2: Euclidean norms of interaction forces/torques. Diagrams 3-8: Euclidean norms of task position errors. The red arrow indicates task deactivation starting from the pointed time; the green arrow marks task activation.

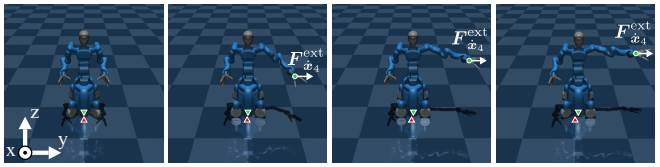

Fig. 5. Simulation #2. Snapshots of Phase #1. The green dot marks the position of the left TCP (task 4), while the red and green triangles indicate the start and actual y-positions of the platform, respectively.

$$\begin{bmatrix} \boldsymbol{T}_A & \boldsymbol{0} \\ \boldsymbol{T}_B & \boldsymbol{T}_C \end{bmatrix}^{-1} = \begin{bmatrix} \boldsymbol{T}_A^{-1} & \boldsymbol{0} \\ -\boldsymbol{T}_C^{-1}\boldsymbol{T}_B\boldsymbol{T}_A^{-1} & \boldsymbol{T}_C^{-1} \end{bmatrix}.$$

The idea is to recursively compute $\boldsymbol{T}_A^{-1}$. Since $\boldsymbol{T}$ in (19) has identities on the diagonal, no matrix inversion is needed.

Algorithm 1 Iterative Computation of $\boldsymbol{B}$

Require: $\boldsymbol{J}_2, \ldots, \boldsymbol{J}_r$; $\bar{\boldsymbol{J}}_1^{\#}, \ldots, \bar{\boldsymbol{J}}_{r-1}^{\#}$
Ensure: $\boldsymbol{B} = \boldsymbol{T}^{-1}$
  $\boldsymbol{B} \leftarrow \boldsymbol{I} \in \mathbb{R}^{\sum_{i=1}^{r} m_i \times \sum_{i=1}^{r} m_i}$
  $\boldsymbol{J}^{\#,\mathrm{aug}} \leftarrow \bar{\boldsymbol{J}}_1^{\#}$
  $\boldsymbol{T}_A^{-1} \leftarrow \boldsymbol{I} \in \mathbb{R}^{m_1 \times m_1}$
  $k \leftarrow m_1$
  for $i = 2 : r$ **do**
    $\boldsymbol{T}_B \leftarrow \boldsymbol{J}_i \boldsymbol{J}^{\#,\mathrm{aug}}$
    $\boldsymbol{T}_C^{-1} \leftarrow \boldsymbol{I} \in \mathbb{R}^{m_i \times m_i}$ (for explanation purposes only)
    $\boldsymbol{B}(k+1 : k+m_i, 1 : k) \leftarrow -\boldsymbol{T}_C^{-1}\boldsymbol{T}_B\boldsymbol{T}_A^{-1}$
    if $i < r$ **then**
      $\boldsymbol{J}^{\#,\mathrm{aug}} \leftarrow [\boldsymbol{J}^{\#,\mathrm{aug}}, \bar{\boldsymbol{J}}_i^{\#}]$
      $k \leftarrow k + m_i$
      $\boldsymbol{T}_A^{-1} \leftarrow \boldsymbol{B}(1 : k, 1 : k)$
    end if
  end for

REFERENCES

[1] Y. Nakamura, H. Hanafusa, and T. Yoshikawa, "Task-priority based redundancy control of robot manipulators," *International Journal of Robotics Research*, vol. 6, no. 2, pp. 3–15, Jun. 1987.

[2] B. Siciliano and J.-J. Slotine, "A general framework for managing multiple tasks in highly redundant robotic systems," in *Proceedings of the 5th International Conference on Advanced Robotics*, Jun. 1991, pp. 1211–1216.

[3] L. Sentis and O. Khatib, "Synthesis of whole-body behaviors through hierarchical control of behavioral primitives," *International Journal of Humanoid Robotics*, vol. 2, no. 4, pp. 505–518, Jan. 2005.

[4] L. Saab, O. E. Ramos, F. Keith, N. Mansard, P. Souères, and J.-I. Fourquet, "Dynamic whole-body motion generation under rigid contacts and other unilateral constraints," *IEEE Transactions on Robotics*, vol. 29, no. 2, pp. 346–362, Apr. 2013.

[5] A. Escande, N. Mansard, and P.-B. Wieber, "Hierarchical quadratic programming: Fast online humanoid-robot motion generation," *International Journal of Robotics Research*, vol. 33, no. 7, pp. 1006–1028, Jun. 2014.

[6] A. D. Prete, F. Romano, L. Natale, G. Metta, G. Sandini, and F. Nori, "Prioritized optimal control," in *Proceedings of IEEE International Conference on Robotics and Automation*, May 2014, pp. 2540–2545.

[7] F. Romano, A. D. Prete, N. Mansard, and F. Nori, "Prioritized optimal control: A hierarchical differential dynamic programming approach," in *Proceedings of IEEE International Conference on Robotics and Automation*, May 2015, pp. 3590–3595.

[8] M. Geisert, A. D. Prete, N. Mansard, F. Romano, and F. Nori, "Regularized hierarchical differential dynamic programming," *IEEE Transactions on Robotics*, vol. 33, no. 4, pp. 819–833, Aug. 2017.

[9] O. Khatib, M. Jorda, J. Park, L. Sentis, and S.-Y. Chung, "Constraint-consistent task-oriented whole-body robot formulation: Task, posture, constraints, multiple contacts, and balance," *The International Journal of Robotics Research*, vol. 41, no. 13-14, pp. 1079–1098, Oct. 2022.

[10] K. Bouyarmane and A. Kheddar, "On weight-prioritized multitask control of humanoid robots," *IEEE Transactions on Automatic Control*, vol. 63, no. 6, pp. 1632–1647, Jun. 2018.

[11] C. Ott, A. Dietrich, and A. Albu-Schäffer, "Prioritized multi-task compliance control of redundant manipulators," *Automatica*, vol. 53, pp. 416–423, Mar. 2015.

[12] A. Dietrich and C. Ott, "Hierarchical impedance-based tracking control of kinematically redundant robots," *IEEE Transactions on Robotics*, vol. 36, no. 1, pp. 204–221, Feb. 2020.

[13] G. Garofalo and C. Ott, "Hierarchical tracking control with arbitrary task dimensions: Application to trajectory tracking on submanifolds," *IEEE Robotics and Automation Letters*, vol. 5, no. 4, pp. 6153–6160, Oct. 2020.

[14] G. Garofalo, X. Wu, and C. Ott, "Adaptive passivity-based multi-task tracking control for robotic manipulators," *IEEE Robotics and Automation Letters*, vol. 6, no. 4, pp. 7129–7136, Oct. 2021.

[15] X. Wu, C. Ott, A. Albu-Schäffer, and A. Dietrich, "Passive decoupled multitask controller for redundant robots," *IEEE Transactions on Control Systems Technology*, vol. 31, no. 1, pp. 1–16, Jan. 2023.

[16] X. Wu, C. Ott, and A. Dietrich, "A comparative experimental study of multi-tasking tracking and interaction control on a torque-controlled humanoid robot," in *Proceedings of American Control Conference*, Jun. 2022, pp. 1933–1940.

[17] K. L. Doty, C. Melchiorri, and C. Bonivento, "A theory of generalized inverses applied to robotics," *International Journal of Robotics Research*, vol. 12, no. 1, pp. 1–19, Feb. 1993.

[18] J. Lachner, F. Allmendinger, S. Stramigioli, and N. Hogan, "Shaping impedances to comply with constrained task dynamics," *IEEE Transactions on Robotics*, vol. 38, no. 5, pp. 2750–2767, Oct. 2022.

[19] F. Keith, P.-B. Wieber, N. Mansard, and A. Kheddar, "Analysis of the discontinuities in prioritized task-space control under discreet task scheduling operations," in *Proceedings of IEEE/RSJ International Conference on Intelligent Robots and Systems*, Sep. 2011, pp. 3887–3892.

[20] A. Dietrich, A. Albu-Schäffer, and G. Hirzinger, "On continuous null space projections for torque-based, hierarchical, multi-objective manipulation," in *Proceedings of IEEE International Conference on Robotics and Automation*, May 2012, pp. 2978–2985.

[21] N. Dehio, D. Kubus, and J. J. Steil, "Continuously shaping projections and operational space tasks," in *Proceedings of IEEE/RSJ International Conference on Intelligent Robots and Systems*, Oct. 2018, pp. 5995–6002.

[22] N. Dehio and J. J. Steil, "Dynamically-consistent generalized hierarchical control," in *Proceedings of International Conference on Robotics and Automation*, May 2019, pp. 1141–1147.

[23] E. Simetti and G. Casalino, "A novel practical technique to integrate inequality control objectives and task transitions in priority based control," *Journal of Intelligent & Robotic Systems*, vol. 84, no. 1-4, pp. 877–902, Apr. 2016.

[24] S. Kim, K. Jang, S. Park, Y. Lee, S. Y. Lee, and J. Park, "Continuous task transition approach for robot controller based on hierarchical quadratic programming," *IEEE Robotics and Automation Letters*, vol. 4, no. 2, pp. 1603–1610, Apr. 2019.

[25] O. Khatib, "A unified approach for motion and force control of robot manipulators: The operational space formulation," *IEEE Journal of Robotics and Automation*, vol. RA-3, no. 1, pp. 43–53, Feb. 1987.

[26] A. Dietrich, C. Ott, and A. Albu-Schäffer, "An overview of null space projections for redundant, torque-controlled robots," *International Journal of Robotics Research*, vol. 34, no. 11, pp. 1385–1400, Sep. 2015.

[27] P. Baerlocher and R. Boulic, "Task-priority formulations for the kinematic control of highly redundant articulated structures," in *Proceedings of IEEE/RSJ International Conference on Intelligent Robots and Systems*, Oct. 1998, pp. 323–329.

[28] L. Righetti, J. Buchli, M. Mistry, and S. Schaal, "Inverse dynamics control of floating-base robots with external constraints: A unified view," in *Proceedings of IEEE International Conference on Robotics and Automation*, May 2011, pp. 1085–1090.

[29] A. Dietrich, *Whole-Body Impedance Control of Wheeled Humanoid Robots*, ser. Springer Tracts in Advanced Robotics. Springer International Publishing, 2016, vol. 116.

[30] N. J. Dehio, "Prioritized multi-objective robot control," Ph.D. dissertation, Technische Universität Carolo-Wilhelmina zu Braunschweig, 2018.

[31] L. Sentis, J. Petersen, and R. Philippsen, "Implementation and stability analysis of prioritized whole-body compliant controllers on a wheeled humanoid robot in uneven terrains," *Autonomous Robots*, vol. 35, no. 4, pp. 301–319, 2013.

[32] B. Henze, A. Dietrich, and C. Ott, "An approach to combine balancing with hierarchical whole-body control for legged humanoid robots," *IEEE Robotics and Automation Letters*, vol. 1, no. 2, pp. 700–707, Jul. 2016.

[33] M. Iskandar, O. Eiberger, A. Albu-Schaffer, A. De Luca, and A. Dietrich, "Collision detection, identification, and localization on the DLR SARA robot with sensing redundancy," in *Proceedings of IEEE International Conference on Robotics and Automation*, May 2021, pp. 3111–3117.

[34] A. De Luca, A. Albu-Schaffer, S. Haddadin, and G. Hirzinger, "Collision detection and safe reaction with the DLR-III lightweight manipulator arm," in *Proceedings of IEEE/RSJ International Conference on Intelligent Robots and Systems*, Oct. 2006, pp. 1623–1630.

[35] L. Sentis, "Synthesis and Control of Whole-Body Behaviors in Humanoid Systems," Ph.D. dissertation, Department of Electrical Engineering, Stanford University, Jul. 2007.

[36] N. Mansfeld, M. Hamad, M. Becker, A. G. Marin, and S. Haddadin, "Safety map: A unified representation for biomechanics impact data and robot instantaneous dynamic properties," *IEEE Robotics and Automation Letters*, vol. 3, no. 3, pp. 1880–1887, Jul. 2018.

[37] N. Mansfeld, G. G. Pena, M. Hamad, A. Kurdas, S. Abdolshah, and S. Haddadin, "Global safety characteristics of wheeled mobile manipulators," in *Proceedings of the 18th IEEE International Conference on Automation Science and Engineering*, Aug. 2022, pp. 2245–2252.

[38] K. Kronander and A. Billard, "Passive interaction control with dynamical systems," *IEEE Robotics and Automation Letters*, vol. 1, no. 1, pp. 106–113, Jan. 2016.

[39] L. Dieci and T. Eirola, "On smooth decompositions of matrices," *SIAM Journal on Matrix Analysis and Applications*, vol. 20, no. 3, pp. 800–819, 1999.

[40] A. Dietrich, K. Bussmann, F. Petit, P. Kotyczka, C. Ott, B. Lohmann, and A. Albu-Schäffer, "Whole-body impedance control of wheeled mobile manipulators: Stability analysis and experiments on the humanoid robot Rollin' Justin," *Autonomous Robots*, vol. 40, no. 3, pp. 505–517, Mar. 2016.

[41] P. R. Giordano, M. Fuchs, A. Albu-Schäffer, and G. Hirzinger, "On the kinematic modeling and control of a mobile platform equipped with steering wheels and movable legs," in *Proceedings of IEEE*

International Conference on Robotics and Automation, May 2009, pp. 4080–4087.

[42] E. Todorov, T. Erez, and Y. Tassa, "MuJoCo: A physics engine for model-based control," in *Proceedings of IEEE/RSJ International Conference on Intelligent Robots and Systems*, Oct. 2012, pp. 5026–5033.

[43] D. Leidner, W. Bejjani, A. Albu-Schäffer, and M. Beetz, "Robotic agents representing, reasoning, and executing wiping tasks for daily household chores," in *Proceedings of International Conference on Autonomous Agents & Multiagent Systems*, May 2016, pp. 1006–1014.

[44] J. Englsberger, G. Mesesan, A. Werner, and C. Ott, "Torque-based dynamic walking - A long way from simulation to experiment," in *Proceedings of IEEE International Conference on Robotics and Automation*, May 2018, pp. 440–447.